



Cite this: DOI: 10.1039/d0dt00543f

# Zn-Templated synthesis of substituted (2,6-diimine)pyridine proligands and evaluation of their iron complexes as anolytes for flow battery applications†

Jason D. Braun,<sup>†</sup> Paul A. Gray,<sup>†</sup> Baldeep K. Sidhu,<sup>†</sup> Dion B. Nemez and David E. Herbert\*

Pseudo-octahedral iron complexes supported by tridentate  $N^*N^*N^*$ -binding, redox 'non-innocent' diiminepyridine (DIP) ligands exhibit multiple reversible ligand-based reductions that suggest the potential application of these complexes as anolytes in redox flow batteries (RFBs). When bearing aryl groups at the imine nitrogens, substitution at the 4-position can be used to tune these redox potentials and impact other properties relevant to RFB applications, such as solubility and stability over extended cycling. DIP ligands bearing electron-withdrawing groups (EWGs) in this position, however, can be challenging to isolate via typical condensation routes involving *para*-substituted anilines and 2,6-diacetylpyridine. In this work, we demonstrate a high-yielding Zn-templated synthesis of DIP ligands bearing strong EWGs. The synthesis and electrochemical characterization of iron(II) complexes of these ligands is also described, along with properties relevant to their potential application as RFB anolytes.

Received 13th February 2020,  
Accepted 9th April 2020

DOI: 10.1039/d0dt00543f

rsc.li/dalton

## Introduction

Redox flow batteries (RFBs) have received renewed attention of late owing to their potential for the scalable, inexpensive storage of the growing proportion of power generation devoted to renewable but intermittent resources such as wind and solar.<sup>1</sup> In an RFB, electrical energy is converted to chemical energy through the electrochemical interconversion of redox pairs serving as the electrolyte.<sup>2</sup> The key contrast with conventional batteries is that these redox pairs can be spatially separated from the electrode.<sup>3</sup> If both oxidized and reduced members of the pairs are stable and soluble in the flow battery medium, scalability will depend in part on the abundance of the materials employed as catholyte/anolyte, and to a more significant extent than on that of the electrode material.<sup>4</sup> With respect to the solvent medium, nonaqueous solvents with wider windows of electrochemical stability can boost the energy density output of an RFB compared to water,<sup>5</sup> though

their cost-competitiveness with aqueous RFBs has been questioned.<sup>6</sup> The increased solubility of many metal coordination complexes (MCCs) in organic solvents, however, does mean a larger library of candidate anolytes and catholytes based on MCCs is available (Fig. 1).<sup>7</sup>

While simple coordination complexes (*e.g.*, **A**; acac = acetylacetonate) exhibit reversible reductions and oxidations that can enable use as both anolyte and catholyte in symmetric RFBs,<sup>8</sup> the introduction of redox 'non-innocent' ligands<sup>9,10</sup> can in principle augment the performance of MCCs in RFBs<sup>11</sup> by providing additional sites for electron-transfer. MCCs of redox non-innocent 2,2'-bipyridine (bpy; **B**)<sup>12</sup> and (bipyridylimino)isoindoline (BPI; **C**)<sup>13</sup> ligands, for example, have been shown

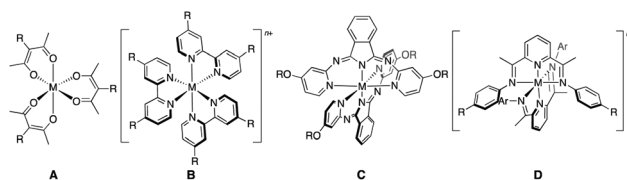


**Fig. 1** Selected examples of metal coordination complexes (MCCs) that have been evaluated for use in non-aqueous redox flow batteries.<sup>6</sup> **A**:  $M(\text{acac})_3$ ,  $M = \text{V, Cr, Mn, Fe, Ru}$ ; acac = acetylacetonate. **B**:  $M(\text{bpy})_3^{n+}$ ,  $M = \text{Ru, Fe, Ni, Cr, Co}$ ; bpy = 2,2'-bipyridine. **C**:  $M(\text{BPI})_2$ ,  $M = \text{Mg, Mn, Fe, Co, Ni, Zn}$ ; BPI = (bipyridylimino)isoindoline. **D**:  $M(\text{DIP})_2^{n+}$ ,  $M = \text{Fe}$ ; DIP = 2,6-diiminepyridine.

Department of Chemistry and the Manitoba Institute for Materials, University of Manitoba, 144 Dysart Road, Winnipeg, Manitoba, R3T 2N2, Canada.

E-mail: david.herbert@umanitoba.ca

† Electronic supplementary information (ESI) available: A PDF containing all spectra, ESI tables of bond distances and angles, and additional electrochemical plots. CIFs for **1b-d** and **3c-d**. CCDC 1983239–1983243. For ESI and crystallographic data in CIF or other electronic format see DOI: 10.1039/d0dt00543f

‡ These authors contributed equally to this work.

to have properties favourable to RFB applications including (for BPI MCCs) multiple electron transfers per molecule, high solubility, and long-term stability towards charge/discharge cycles (~200) with very little capacity fade.<sup>13</sup> For comparison, one of the more commercially promising systems is the all-vanadium flow battery, which utilizes four different oxidation state vanadium and oxyvanadium ions and shows very impressive long-term cyclability of over 1000 stable cycles.<sup>14</sup> The high system costs comprised to a large extent of the cost of the redox-active material, however, still far exceed the U.S. Department of Energy's target.<sup>15</sup>

In this context, we have been interested in the application of iron coordination complexes of a popular class of redox non-innocent scaffold, 2,6-diiminepyridines (DIP),<sup>16</sup> which are able to accommodate up to three additional electrons in s-,<sup>17</sup> f-<sup>18</sup> and d-block<sup>19</sup> metal complexes of triply reduced DIPs. Pseudo-octahedral iron complexes of *N*-aryl DIPs bearing electron-releasing substituents (**D**, R = *t*Bu or OMe, M = Fe, *n* = 2), for example, exhibit good solubility (0.1–0.3 M) in CH<sub>3</sub>CN and two reversible reductions at negative potentials beyond the water voltage window.<sup>16</sup> Such molecular geometries also make use of tridentate DIP chelation which limits ligand dissociation and promotes higher cyclability compared to bidentate ligand environments; 2,6-unsubstituted aryl groups similarly reduce ligand hemilability associated with steric congestion.<sup>20</sup> We have also found that, in addition to the position of the reduction potentials, the solubility and stability towards cycling were also impacted by the identity of the substituent in the 4-position of *N*-phenyl rings. Complexes of DIP ligands bearing *t*Bu substituents showed improved capacity retention attributed to enhanced solubility of both reduced and oxidized species.<sup>16</sup> As *t*Bu and OMe are both electron-releasing, we thought to explore the impact electron-withdrawing groups (EWGs) might have on reduction potentials and cycling stability in the context of RFB anolytes.

Installation of *para*-EWGs on the flanking aryl substituents in DIP frameworks, however, is potentially more problematic than electron-donating groups (EDGs). DIPs are typically prepared by condensation of 2,6-diacetylpyridine and the corresponding anilines. Substitution of anilines in the 4-position with EWGs can significantly reduce their nucleophilicity, hampering conversion.<sup>21</sup> For example, condensation syntheses of (*para*-fluoro)phenyl and (*para*-bromo)phenyl-substituted DIPs are reported to give isolated yields of only 24% and 41%, respectively, despite azeotropic removal of water.<sup>21</sup> Furthermore, the *para*-nitro analogue could only be isolated, and in similarly low yields, following a five day, acid-catalyzed Dean–Stark reflux in high-boiling *p*-xylene.<sup>22</sup> In seeking to overcome these challenges, we considered a report on the inclusion of EWGs on <sup>Ar</sup>BIAN-type diimine ligands *via* a Zn-templated synthesis (<sup>Ar</sup>BIAN = bis(aryl)acenaphthenequinone-diimine).<sup>23</sup> Here, we describe the application of this approach to the synthesis of DIP ligands with strong EWGs in relatively high yields under mild conditions. This methodology opens the chemical space for the synthesis of DIP ligands that incorporate strong EWGs and so may be useful for the many appli-

cations where these ligands are utilized.<sup>24</sup> We furthermore report on the electrochemical evaluation of properties of their pseudo-octahedral Fe(II) complexes which speak to potential use as anolytes in RFB applications.

## Results and discussion

### Synthesis and characterization of ligands and complexes

DIP proligand synthesis is generally accomplished by the acid-catalyzed condensation of 2,6-diacetylpyridine with two equivalents of the appropriately substituted aniline. To avoid forcing conditions required for appreciable conversion using anilines substituted in the 4-position with electron-withdrawing groups (EWGs), we turned to templated synthesis. Templated ligand syntheses have long been used to overcome competing side reactions,<sup>25</sup> but can also be used to drive to completion ligand formation reactions that would suffer from less favourable thermodynamics in the absence of coordination to a templating metal ion.<sup>26</sup> The templated synthesis of imine-based ligands, for example, has enabled construction of complex scaffolds including chiral *P*<sup>^</sup>*N*<sup>^</sup>*N* and *P*<sup>^</sup>*N*<sup>^</sup>*N*<sup>^</sup>*P* multidentate architectures.<sup>27</sup> In comparison, reports of demetallation and subsequent use of the liberated proligands appear far less often<sup>28</sup> than the targeted assembly of coordination complexes templated by a metal ion of choice. For imines, attempts to demetallate can lead to ligand hydrolysis. In the case of <sup>Ar</sup>BIAN ligands constructed around Zn<sup>2+</sup> as a templating ion, using oxalate (C<sub>2</sub>O<sub>4</sub><sup>2-</sup>) as a displacing ligand produces insoluble ZnC<sub>2</sub>O<sub>4</sub> and drives demetallation reactions to completion without evidence of hydrolysis.<sup>23</sup>

Four (DIP)ZnCl<sub>2</sub> complexes (**1a–d**, Fig. 2) were prepared *via* the Zn<sup>2+</sup>-templated condensation of two equivalents of aniline with 2,6-diacetylpyridine, broadly following the protocol for incorporating strong EWGs in <sup>Ar</sup>BIANs outlined by Ragaini.<sup>23</sup> Complex **1a** (R = H) has been previously reported.<sup>29</sup> Each of **1a–d** was prepared in this way by heating slightly more than two equivalents of the appropriate aniline (15% excess) with 2,6-diacetylpyridine and excess ZnCl<sub>2</sub> in CH<sub>3</sub>OH (acetic acid for **1d**). Unlike complexes based on the acenaphthoquinone

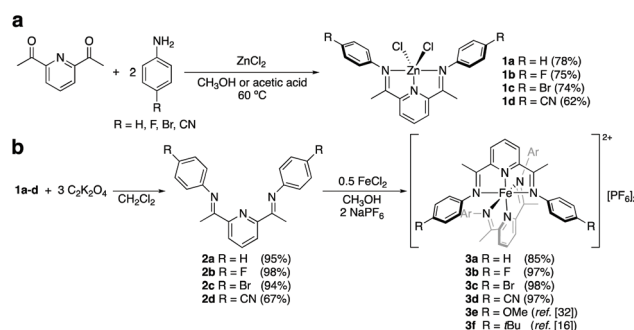


Fig. 2 Synthesis of (a) (DIP)ZnCl<sub>2</sub> complexes **1a–d**; (b) free proligands **2a–d** *via* de-zincation, and [bis(DIP)<sub>2</sub>Fe][PF<sub>6</sub>]<sub>2</sub> complexes **3a–d** with isolated yields in parentheses. Complexes **3e** (ref. 32) and **3f** (ref. 16) have been previously reported.

(<sup>Ar</sup>BIAN) backbone,<sup>23</sup> using acetic acid as the solvent leads to full solubilization of the (DIP)ZnCl<sub>2</sub> fluoro- and bromo-derivatives, but partial solubilization of the cyano-derivative. Changing the reaction solvent to methanol, the crude (DIP)ZnCl<sub>2</sub> product precipitates as a yellow powder upon cooling to room temperature and can be filtered to easily separate **1a–c** from excess reactants. The (DIP)ZnCl<sub>2</sub> complexes can then be recrystallized by dissolving in hot acetonitrile, followed by slow cooling to –20 °C. <sup>1</sup>H NMR spectra for **1a–d** show a single, pseudo C<sub>2v</sub>-symmetric magnetic environment in solution for all four Zn complexes. Diagnostic resonances for the formation of the imine arms can also be observed by <sup>13</sup>C{<sup>1</sup>H} NMR at δ = ~165 ppm. The molecular formula for each compound was confirmed by high-resolution mass spectrometry (HR-MS).

To confirm the structures of the (DIP)ZnCl<sub>2</sub> complexes suggested by solution NMR and HR-MS, solid-state structures of **1b–d** were also determined by single-crystal X-ray diffraction (XRD; Fig. 3). In each case, a single DIP ligand is bound to Zn in a meridional, tridentate fashion and forms part of what is best described as a distorted square-based pyramid with τ<sub>5</sub> values<sup>30</sup> ranging from 0.30 (**1c**) to 0.40 (**1d**). This deviation from ideal geometry arises from different N<sub>pyr</sub>–Zn–Cl angles. The two chlorides cant asymmetrically away from the pyridine ring, opening one N<sub>pyr</sub>–Zn–Cl angle wider than the other. The relatively long Zn–N<sub>pyr</sub> and Zn–N<sub>imine</sub> distances, typical of (N-heterocycle/imine)-Zn<sup>2+</sup> coordination,<sup>31</sup> are consistent across the series **1b–d** at ~2.08 Å and 2.21–2.26 Å, respectively. As a result, the N<sub>imine</sub>–Zn–N<sub>imine</sub> angles are quite pulled back (147–148°). The narrow range of bond distances and angles observed for the set of (DIP)ZnCl<sub>2</sub> complexes is consistent with the distal placement of the R groups on the ligand periphery.

The free proligands (**2a–d**) can be displaced from the ZnCl<sub>2</sub> unit and isolated in good to excellent yields (67–98%) by mixing dichloromethane solutions of **1a–d** with aqueous solutions containing three equivalents of potassium oxalate, then extracting and drying the organic layer. Multinuclear NMR confirmed the molecular composition of the resulting off-white/yellow solids as demetallated ligand, with shifts observed to all signals including those attributed to the diagnostic imine carbon nuclei (δ<sub>C=N</sub> = ~168 ppm). Iron MCCs **3a–d** were subsequently prepared by reaction of the desired proli-

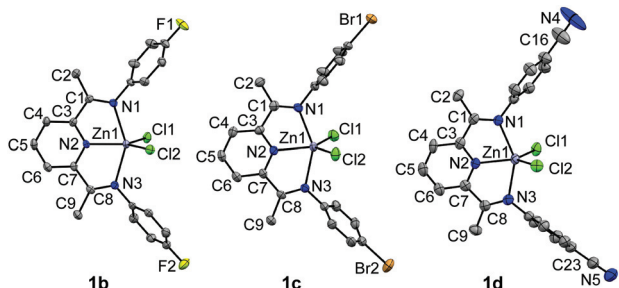


Fig. 3 Solid-state X-ray diffraction structures of **1b**, **1c** and **1d** shown with ellipsoids at the 50% probability level. Hydrogen atoms and solvent molecules are omitted for clarity. Selected bond lengths and angles reported in Tables S1 and S2.†

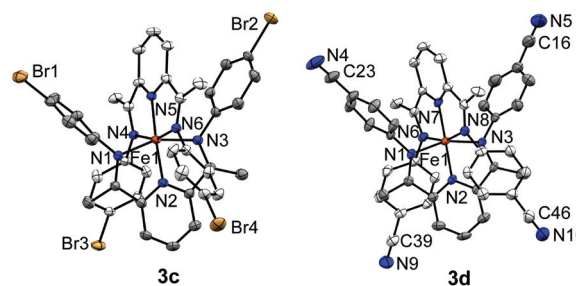


Fig. 4 Solid-state X-ray diffraction structures of **3c** and **3d**, shown with ellipsoids at the 50% probability level. Hydrogen atoms, counterions and solvent molecules are omitted for clarity. Selected bond lengths and angles reported in Tables S1 and S2.†

gand with 0.5 equivalents of anhydrous FeCl<sub>2</sub> and two equivalents of NaPF<sub>6</sub> in CH<sub>3</sub>OH. These complexes were isolated as air- and moisture-stable, deep purple solids, with molecular formulae again confirmed by HR-MS. Multinuclear NMR suggests a symmetric environment around each Fe(II) centre with <sup>13</sup>C resonances for the diagnostic imine carbon centers shifted considerably downfield to δ<sub>C=N</sub> ~180 ppm. The most downfield resonance is observed for **3d** (δ<sub>C=N</sub> = 182 ppm), consistent with **3d** having the most deshielded imine carbon. The dark purple colour of **3a–d** is reflected in strong and broad low energy features in the steady-state UV-Vis absorption spectra (Fig. S37†). These transitions are assigned as MLCT in character, as is typical of [(DIP)<sub>2</sub>Fe]<sup>2+</sup> complexes.<sup>16,32</sup> Within the series, **3d** showed a marked hypsochromic shift in the transitions observed beyond 400 nm, but otherwise, a similar absorption profile is observed for all four complexes. The pseudo-octahedral coordination environment around Fe was confirmed by XRD studies of **3c** and **3d** (Fig. 4). A much tighter coordination environment is seen for the Fe complexes compared with the Zn congeners (Tables S1 and S2†), with closer M–N distances ranging from 1.86–1.87 Å for Fe–N<sub>pyr</sub> and 1.96–2.00 Å for Fe–N<sub>imine</sub>. As a result, the intraligand N<sub>imine</sub>–Fe–N<sub>imine</sub> angles are much larger at ~160°.

Cyclic voltammetry (CV) and differential pulse voltammetry (DPV; Fig. 5 and Table 1) revealed identical redox behaviour for the series **3a–d**, with two reversible 1e<sup>–</sup> reductions evident between –1.0 and –2.0 V and a 1e<sup>–</sup> oxidation observed near +1.0 V vs. FcH<sup>0/+</sup> (FcH = ferrocene). Based on previous analysis of the redox behaviour of DIP complexes of Fe, we assign the cathodic events as ligand centered.<sup>32</sup> The oxidation is attributed to a metal-centered Fe<sup>2+/3+</sup> couple. Each of the three redox events observed for **3a–d** are shifted anodically compared to those observed for [(DIP)Fe]<sup>2+</sup> analogs bearing electron-releasing OMe (**3e**) or *t*Bu (**3f**) substituents.<sup>16</sup> This highlights the ability to tune redox potentials using distal substitution of the *N*-arene rings. In accordance with their Hammett parameters,<sup>33</sup> the largest anodic shift is observed for R = CN, followed by R = Br and R = F, consistent with inductive removal of electron density from the imine-based LUMO. The reversibility of the ligand-based reductions observed by CV does not seem to be as adversely affected by the introduction of EWGs

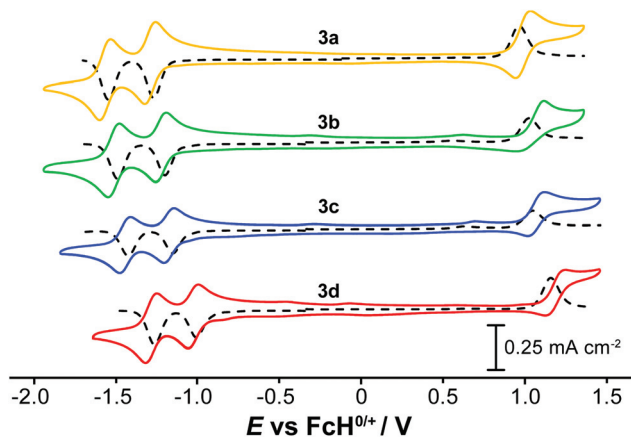


Fig. 5 CV/DPVs of **3a–d** (0.6 mM of analyte, 0.1 M  $n\text{Bu}_4\text{PF}_6$  in  $\text{CH}_3\text{CN}$ , GCE, scan rate =  $100 \text{ mV s}^{-1}$ ).

Table 1 Electrochemical and RFB parameters for **3a–f**<sup>a</sup>

	$E_{1/2}/\text{V}$	$\Delta_{\text{ptp}}/\text{mV}$	$i_{\text{red}}/i_{\text{ox}}$	CE/%	FE/%	$e^-/\text{mol}$
<b>3a</b>	-1.55	67	0.88	95.2	93.4	1.9
	-1.27	65	1.14			
	0.97	82	0.86			
<b>3b</b>	-1.49	69	0.90	84.8	61.2	1.2
	-1.20	66	1.16			
	1.03	158	0.23			
<b>3c</b>	-1.43	65	0.86	95.2	24.6	0.5
	-1.15	59	1.23			
	1.05	103	0.68			
<b>3d</b>	-1.26	68	0.87	85.0	42.6	0.9
	-1.01	62	1.31			
	1.16	138	0.68			
<b>3e<sup>b</sup></b>	-1.60	75	0.97	94.3	70.0	1.4
	-1.30	61	0.99			
	0.86	77	0.97			
<b>3f<sup>b</sup></b>	-1.59	60	1.04	>99.9	82.1	1.6
	-1.32	60	0.95			
	0.90	69	0.97			

<sup>a</sup> Average coulombic efficiency (CE), average faradaic efficiency (FE) taken by averaging charging and discharging FE, and average number of electrons cycled taken by averaging number of electrons cycled upon charging and discharging. <sup>b</sup> Values taken from ref. 16.

as the  $\text{Fe}^{2+/3+}$  couples, which are much more reversible for **3e–f** likely as a result of occurring at less positive potentials.<sup>16</sup> In particular, both cathodic events show peak current ratios near to unity and narrow peak-to-peak separations close to the Nernstian limit of 59 mV.<sup>34</sup> Moreover, the potentials surpass the voltage limits of water (*ca.*  $-1.2 \text{ V vs. FcH}^{0/+}$ )<sup>35</sup> and the multiple electron transfers possible with a single complex suggest the possibility of high energy storage capacity.<sup>13</sup> We therefore proceeded to evaluate the suitability of **3a–d** as RFB analytes.

### Charge/discharge measurements

Cycling measurements were performed on **3a–d** using a reticulated vitreous carbon (RVC) working electrode in a bulk electrolysis cell to examine the viability of these compounds as RFB analytes. The maximum cathodic potentials were set according to the CV/DPV collected for each compound to

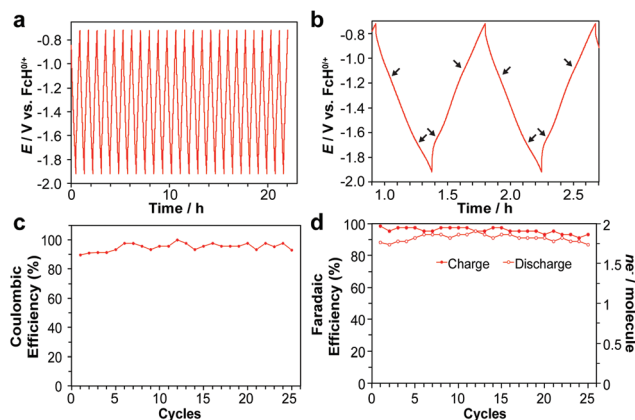


Fig. 6 (a and b) Total cell voltage, (c) coulombic efficiency (% CE), and (d) capacity retention for **3a**. Anodic and cathodic current set to 7 mA with a charging rate of 1 C. Voltage limits set according to previously obtained CVs in order to limit accessing irreversible redox events; in 0.3 M  $n\text{Bu}_4\text{PF}_6$  acetonitrile solution. Plateaus are marked by arrows.

ensure capture of the second reversible redox event without going so far as to irreversibly reduce the complexes.<sup>16</sup> The charge/discharge cycling experiments for **3a** are shown in Fig. 6. While less pronounced than those observed for **3e–f**,<sup>16</sup> plateaus corresponding to the reduction events observed by CV/DPV can be discerned in the charging segment. In the discharge segment, two plateaus corresponding to the reverse oxidation events can similarly be noted (Fig. 6b). These decrease in prominence after extended cycling.

The cycling stability of RFB electrolytes is one of a number of parameters important for evaluating the potential for use in a commercial battery.<sup>36</sup> Through 25 cycles, **3a** exhibits a coulombic efficiency (% CE) of 95.2% (Fig. 6c), comparable to reported values for aqueous Li/I RFBs over 20 cycles,<sup>37</sup> but passing an average of  $\sim 1.9$  electrons per molecule out of a theoretical maximum of 2 (Fig. 6d and Table 1). Zn–I flow batteries, in comparison have been reported to exhibit extended stability over 300 cycles, with a one-electron redox couple.<sup>38</sup> In comparison to complexes bearing donating groups (**3e–f**),<sup>16</sup> **3a** surpasses the faradaic efficiency (% FE) and number of electrons per molecule observed for **3e–f** without any evidence of degradation. For **3b–d**, over the course of extended cycling, the cycles become narrower resulting in reduced overall efficiency parameters (Table 1 and Fig. S42–S44<sup>†</sup>). We note the potentials for reduction of organic aryl halides and nitriles<sup>39</sup> fall close to those observed for the reductions of **3a–d**. Over time, irreversible chemical reduction of these groups may contribute an underlying degradation pathway for the ligands that include these substituents. Indeed, slightly less Nernstian peak parameters are observed by CV for **3e–d** (Table 1).

## Conclusions

This work presents a facile synthetic route for the incorporation of strong EWGs into the *para* position of the flanking

aryl substituents on DIP ligands. This Zn-templated methodology offers higher yields, shortened reaction times and requires considerably milder conditions than previously reported for analogous DIPs,<sup>21,22</sup> expanding the chemical scope available in the construction of these increasingly widely used ligands.<sup>40</sup> Isolation of DIP ligands bearing strong EWGs has also enabled the high-yielding synthesis of new [(DIP)<sub>2</sub>Fe]<sup>2+</sup> salts **3b–d**, along with novel, structurally characterized examples of (DIP)ZnCl<sub>2</sub> complexes **1a–d**. Regarding the potential application of **3a–d** in RFBs, **3a** is shown to be a viable candidate as an RFB anolyte, displaying stability over at least 25 cycles while maintaining access to multiple electrons equivalents per molecule (~1.9) over this range, surpassing previously reported examples **3e–f**.<sup>16</sup> The use of halides or pseudohalides at the ligand periphery, however, was found to be detrimental to cycling performance. This observation should help guide future ligand designs for MCCs for RFB applications.

## Experimental section

Unless otherwise specified, all air sensitive manipulations were carried out either in a N<sub>2</sub> filled glove box or using standard Schlenk techniques under Ar. ZnCl<sub>2</sub> (Alfa Aesar), 4-fluoroaniline (Combi Blocks), 4-bromoaniline (Acros Organics), aniline (Sigma Aldrich), 4-aminobenzonitrile (Combi Blocks), 2,6-diacetylpyridine (Combi Blocks), K<sub>2</sub>[C<sub>2</sub>O<sub>4</sub>] (Alfa Aesar), FeCl<sub>2</sub> (Acros Organics), NaPF<sub>6</sub> (Alfa Aesar), acetic acid and methanol (Fisher Scientific) were purchased and used without any further purification. Organic solvents used for electrochemical tests were dried and distilled using appropriate drying agents prior to use. 1- and 2D NMR spectra were recorded on Bruker Avance 300 MHz or Bruker Avance – III 500 MHz spectrometers. <sup>1</sup>H and <sup>13</sup>C{<sup>1</sup>H} NMR spectra were referenced to residual solvent peaks. Mass spectrometry (ESI-TOF/MS), was performed at the University of Manitoba on a Bruker Compact LC-ESI-TOF/MS analyzer. Electronic absorption spectra were recorded on an Agilent Technologies Cary 5000 Series UV-Vis-NIR spectrophotometer in dual beam mode.

### 2,6-Bis(phenylimino)pyridine zinc dichloride (**1a**)

In a thick-walled flask, ZnCl<sub>2</sub> (0.250 g, 1.83 mmol) and 2,6-diacetylpyridine (0.102 g, 0.627 mmol) were combined with methanol (2.5 mL) giving a colourless precipitate. This mixture was heated to 60 °C, and aniline (0.134 g, 1.43 mmol; 0.13 mL) added to the hot solution. The flask was then sealed with a Teflon stopper and heated to 90 °C for 4 h behind a blast shield. A yellow precipitate was formed upon cooling to room temperature and collected by filtration. The solid product was recrystallized from acetonitrile and washed with chloroform to give a light-yellow powder. Isolated yield: 0.220 g (78%). <sup>1</sup>H NMR (CD<sub>3</sub>CN, 500 MHz, 25 °C): δ 8.53 (m, 1H; PyrH<sub>p</sub>), 8.41 (m, 2H; PyrH<sub>m</sub>), 7.45 (m, 4H; ArH), 7.29 (m, 2H; ArH), 7.21 (m, 4H; ArH), 2.46 ppm (s,

6H; N=CMe). <sup>13</sup>C{<sup>1</sup>H} NMR (CD<sub>3</sub>CN, 125 MHz, 25 °C): δ 164.9 (MeC=N), 149.7 (C<sub>Ar</sub>), 147.6 (C<sub>Ar</sub>), 144.9 (C<sub>Ar</sub>), 129.6 (C<sub>Ar</sub>), 128.1 (C<sub>Ar</sub>), 126.9 (C<sub>Ar</sub>), 122.8 (C<sub>Ar</sub>), 17.4 ppm (CH<sub>3</sub>). MS (ESI-TOF/MS, *m/z*) calcd for C<sub>21</sub>H<sub>19</sub>ClN<sub>3</sub>Zn [M]<sup>+</sup>, 412.0553; found 412.0550.

### 2,6-Bis(4-fluorophenylimino)pyridine zinc dichloride (**1b**)

Procedure as for **1a** using: ZnCl<sub>2</sub> (0.250 g, 1.83 mmol), 2,6-diacetylpyridine (0.103 g, 0.631 mmol), methanol (2.5 mL), and 4-fluoroaniline (0.164 g, 1.48 mmol; 0.14 mL). Light-yellow powder. Isolated yield: 0.230 g (75%). <sup>1</sup>H NMR (CD<sub>3</sub>CN, 500 MHz, 25 °C): δ 8.54 (m, 1H; PyrH<sub>p</sub>), 8.41 (m, 2H; PyrH<sub>m</sub>), 7.25 (m, 4H; ArH), 7.19 (m, 4H; ArH), 2.47 ppm (s, 6H; N=CMe). <sup>13</sup>C{<sup>1</sup>H} NMR (CD<sub>3</sub>CN, 125 MHz, 25 °C, ppm): δ 165.6 (MeC=N), 161.8 (d, J<sub>CF</sub> = 241.3 Hz; C<sub>Ar</sub>), 149.7 (C<sub>Ar</sub>), 144.9 (C<sub>Ar</sub>), 143.7 (d, J<sub>CF</sub> = 3.75 Hz; C<sub>Ar</sub>), 128.2 (C<sub>Ar</sub>), 124.8 (d, J<sub>CF</sub> = 7.5 Hz; C<sub>Ar</sub>), 116.3 (d, J<sub>CF</sub> = 23.8 Hz; C<sub>Ar</sub>), 17.5 ppm (CH<sub>3</sub>). <sup>19</sup>F{<sup>1</sup>H} NMR (CD<sub>3</sub>CN, 282 MHz, 25 °C): δ –118.9 ppm (s). MS (ESI-TOF/MS, *m/z*) calcd for C<sub>21</sub>H<sub>17</sub>ClN<sub>3</sub>ZnF<sub>2</sub> [M]<sup>+</sup>, 448.0365; found 448.0367.

### 2,6-Bis(4-bromophenylimino)pyridine zinc dichloride (**1c**)

Procedure as for **1a** using: ZnCl<sub>2</sub> (1.00 g, 7.32 mmol), 2,6-diacetylpyridine (0.398 g, 2.44 mmol) methanol (8 mL) and 4-bromoaniline (0.880 g, 5.12 mmol). Light brown powder. Isolated yield: 1.10 g (74%). <sup>1</sup>H NMR (CD<sub>3</sub>CN, 300 MHz, 25 °C): δ 8.54 (m, 1H; PyrH<sub>p</sub>), 8.42 (m, 2H; PyrH<sub>m</sub>), 7.60 (m, 4H; ArH), 7.15 (m, 4H; ArH), 2.47 ppm (s, 6H; N=CMe). <sup>13</sup>C{<sup>1</sup>H} NMR (CD<sub>3</sub>CN, 125 MHz, 25 °C): δ 165.6 (MeC=N), 149.3 (C<sub>Ar</sub>), 146.4 (C<sub>Ar</sub>), 144.8 (C<sub>Ar</sub>), 132.5 (C<sub>Ar</sub>), 128.1 (C<sub>Ar</sub>), 124.7 (C<sub>Ar</sub>), 119.7 (C<sub>Ar</sub>), 17.4 ppm (CH<sub>3</sub>). MS (ESI-TOF/MS, *m/z*) calcd for C<sub>21</sub>H<sub>17</sub>ClN<sub>3</sub>ZnBr<sub>2</sub> [M]<sup>+</sup>, 567.8764; found 567.9041.

### 2,6-Bis(4-cyanophenylimino)pyridine zinc dichloride (**1d**)

In a thick-walled flask, ZnCl<sub>2</sub> (1.00 g, 7.34 mmol) and 2,6-diacetylpyridine (0.440 g, 2.70 mmol) were combined with acetic acid (8 mL) giving a colourless precipitate. This mixture was heated to 60 °C and 4-aminobenzonitrile (0.744 g, 6.3 mmol) added to the hot solution. The flask was then sealed with a Teflon stopper and heated to 130 °C for 3 h behind a blast shield. A yellow precipitate was formed upon cooling to room temperature and collected by filtration. The solid was suspended in diethyl ether and stirred for 10 min. This suspension was filtered and the collected solid washed with an additional 3 × 15 mL of diethyl ether, then dried *in vacuo*. Yellow solid. Isolated yield: 0.836 g (62%). <sup>1</sup>H NMR (CD<sub>3</sub>CN, 300 MHz, 25 °C): δ 8.60 (m, 1H; PyrH<sub>p</sub>), 8.48 (m, 2H; PyrH<sub>m</sub>), 7.81 (m, 4H; ArH), 7.32 (m, 4H; ArH), 2.46 ppm (s, 6H; N=CMe). <sup>13</sup>C{<sup>1</sup>H} NMR (CD<sub>3</sub>CN, 75 MHz, 25 °C): δ 167.4 (MeC=N), 151.0 (C<sub>Ar</sub>), 149.0 (C<sub>Ar</sub>), 145.5 (C<sub>Ar</sub>), 134.1 (C<sub>Ar</sub>), 128.8 (C<sub>Ar</sub>), 123.6 (C<sub>Ar</sub>), 119.4 (C≡N), 110.4 (C<sub>Ar</sub>), 17.9 ppm (CH<sub>3</sub>). MS (ESI-TOF/MS, *m/z*) calcd for C<sub>23</sub>H<sub>17</sub>ClN<sub>5</sub>Zn [M]<sup>+</sup>, 462.0458; found 462.0447.

### General procedure for the isolation of decoordinated proligands

Zn complexes **1a-d** (1 mmol) were each suspended in CH<sub>2</sub>Cl<sub>2</sub> (50 mL) in a separatory funnel. An aqueous solution (20 mL) of potassium oxalate (3 mmol) was then added and the mixture was shaken for 5 min, giving a cloudy aqueous layer over a yellow organic layer. The organic layer was washed with an additional 2 × 30 mL of water, stirred over Na<sub>2</sub>SO<sub>4</sub>, and the volatiles removed under reduced pressure.

**2,6-Bis(phenylimino)pyridine (2a).** Isolated yield: 0.298 g (95%). <sup>1</sup>H NMR (CDCl<sub>3</sub>, 300 MHz, 25 °C): δ 8.35 (d, 2H, *J*<sub>HH</sub> = 7.8 Hz; Pyr*H*<sub>m</sub>), 7.88 (t, 1H, *J*<sub>HH</sub> = 7.8 Hz; Pyr*H*<sub>p</sub>), 7.39 (t, 4H, *J*<sub>HH</sub> = 7.9 Hz; Ar*H*), 7.13 (m, 2H; Ar*H*), 7.85 (m, 4H; Ar*H*), 2.41 ppm (s, 6H; N=CMe). <sup>13</sup>C{<sup>1</sup>H} NMR (CDCl<sub>3</sub>, 75 MHz, 25 °C): δ 167.5 (MeC=N), 155.6 (C<sub>Ar</sub>), 151.4 (C<sub>Ar</sub>), 137.0 (C<sub>Ar</sub>), 129.2 (C<sub>Ar</sub>), 123.8 (C<sub>Ar</sub>), 122.4 (C<sub>Ar</sub>), 119.4 (C<sub>Ar</sub>), 16.4 ppm (CH<sub>3</sub>).

**2,6-Bis(4-fluorophenylimino)pyridine (2b).** Isolated yield: 0.342 g (98%). <sup>1</sup>H NMR (CDCl<sub>3</sub>, 300 MHz, 25 °C): δ 8.32 (d, 2H, *J*<sub>HH</sub> = 7.8 Hz; Pyr*H*<sub>m</sub>), 7.88 (t, 1H, *J*<sub>HH</sub> = 7.8 Hz; Pyr*H*<sub>p</sub>), 7.08 (m, 4H; Ar*H*), 6.81 (m, 4H; Ar*H*), 2.41 ppm (s, 6H; N=CMe). <sup>13</sup>C{<sup>1</sup>H} NMR (CDCl<sub>3</sub>, 75 MHz, 25 °C): δ 168.2 (MeC=N), 159.7 (d, *J*<sub>CF</sub> = 241.2 Hz; F-C<sub>Ar</sub>), 155.5 (C<sub>Ar</sub>), 147.3 (d, *J*<sub>CF</sub> = 2.8 Hz; C<sub>Ar</sub>), 137.0 (C<sub>Ar</sub>), 122.5 (C<sub>Ar</sub>), 120.9 (d, *J*<sub>CF</sub> = 7.9 Hz; C<sub>Ar</sub>), 115.8 (d, *J*<sub>CF</sub> = 22.5 Hz; C<sub>Ar</sub>), 16.4 ppm (CH<sub>3</sub>). <sup>19</sup>F{<sup>1</sup>H} NMR (CDCl<sub>3</sub>, 282 MHz, 25 °C): δ -120.5 ppm (s).

**2,6-Bis(4-bromophenylimino)pyridine (2c).** Isolated yield: 0.443 g (94%). <sup>1</sup>H NMR (CDCl<sub>3</sub>, 300 MHz, 25 °C): δ 8.32 (d, 2H, *J*<sub>HH</sub> = 7.8 Hz; Pyr*H*<sub>m</sub>), 7.88 (t, 1H, *J*<sub>HH</sub> = 7.8 Hz; Pyr*H*<sub>p</sub>), 7.49 (m, 4H; Ar*H*), 6.73 (m, 4H; Ar*H*), 2.39 ppm (s, 6H; N=CMe). <sup>13</sup>C{<sup>1</sup>H} NMR (CDCl<sub>3</sub>, 75 MHz, 25 °C): δ 168.1 (MeC=N), 155.3 (C<sub>Ar</sub>), 150.3 (C<sub>Ar</sub>), 137.1 (C<sub>Ar</sub>), 132.2 (C<sub>Ar</sub>), 122.7 (C<sub>Ar</sub>), 121.3 (C<sub>Ar</sub>), 116.8 (C<sub>Ar</sub>), 16.4 ppm (CH<sub>3</sub>).

**2,6-Bis(4-cyanophenylimino)pyridine (2d).** Isolated yield: 0.243 g (67%). <sup>1</sup>H NMR (CDCl<sub>3</sub>, 300 MHz, 25 °C): δ 8.34 (d, 2H, *J*<sub>HH</sub> = 9.0 Hz; Pyr*H*<sub>m</sub>), 7.93 (t, 1H, *J*<sub>HH</sub> = 7.5 Hz; Pyr*H*<sub>p</sub>), 7.68 (d, 4H, *J*<sub>HH</sub> = 6.0 Hz; Ar*H*), 6.92 (d, 4H, *J*<sub>HH</sub> = 9.0 Hz; Ar*H*), 2.39 ppm (s, 6H; N=CMe). <sup>13</sup>C{<sup>1</sup>H} NMR (CDCl<sub>3</sub>, 75 MHz, 25 °C): δ 168.0 (MeC=N), 155.3 (C<sub>Ar</sub>), 154.8 (C<sub>Ar</sub>), 137.3 (C<sub>Ar</sub>), 133.5 (C<sub>Ar</sub>), 123.2 (C<sub>Ar</sub>), 120.0 (C<sub>Ar</sub>), 119.3 (C≡N), 107.2 (C<sub>Ar</sub>), 16.7 ppm (CH<sub>3</sub>).

### Synthesis of iron complexes

**Bis[2,6-bis(phenylimino)pyridine] iron(II) hexafluorophosphate (3a).** A 100 mL flask was charged with **2a** (0.125 g, 0.40 mmol) and FeCl<sub>2</sub> (0.25 g, 0.20 mmol) under N<sub>2</sub>. Degassed methanol (30 mL) was added *via* cannula, immediately forming a dark purple solution. The solution was stirred for 30 min and solid NaPF<sub>6</sub> (0.101 g, 0.60 mmol) was added. The solution was stirred for an additional 30 min, and the volatiles were removed under reduced pressure. Water (20 mL) was added and the mixture was triturated, filtered, and washed with an addition 3 × 5 mL of water, leaving a dark purple solid. This solid was collected and dried *in vacuo*. Isolated yield: 0.165 g (85%). <sup>1</sup>H NMR (CD<sub>3</sub>CN, 300 MHz, 25 °C): δ 8.11 (m, 3H; Pyr*H*<sub>m</sub> and Pyr*H*<sub>p</sub>), 7.18 (m, 6H; Ar*H*), 6.21 (m, 4H;

Ar*H*), 2.56 ppm (s, 6H; N=CMe). <sup>13</sup>C{<sup>1</sup>H} NMR (CD<sub>3</sub>CN, 75 MHz, 25 °C): δ 179.6 (MeC=N), 160.2 (C<sub>Ar</sub>), 144.3 (C<sub>Ar</sub>), 136.8 (C<sub>Ar</sub>), 130.8 (C<sub>Ar</sub>), 128.7 (C<sub>Ar</sub>), 127.9 (C<sub>Ar</sub>), 120.2 (C<sub>Ar</sub>), 19.6 ppm (CH<sub>3</sub>). <sup>19</sup>F NMR (CD<sub>3</sub>CN, 282 MHz, 25 °C): δ -72.9 ppm (d, *J*<sub>PF</sub> = 705.4 Hz; PF<sub>6</sub>). <sup>31</sup>P{<sup>1</sup>H} NMR (CD<sub>3</sub>CN, 121 MHz, 25 °C): δ -144.7 (q, *J*<sub>FP</sub> = 706.7 Hz; PF<sub>6</sub>). Anal. calcd for C<sub>42</sub>H<sub>38</sub>N<sub>6</sub>F<sub>12</sub>P<sub>2</sub>Fe: C, 51.87; H, 3.94. Found: C, 52.26; H, 4.02. MS (ESI-TOF/MS, *m/z*) calcd for C<sub>42</sub>H<sub>38</sub>N<sub>6</sub>Fe [M + H]<sup>+</sup>, 681.2424; found 681.2439.

**Bis[2,6-bis(4-fluorophenylimino)pyridine] iron(II) hexafluorophosphate (3b).** Procedure as for **3a** using: **2b** (0.14 g, 0.40 mmol) and FeCl<sub>2</sub> (0.25 g, 0.20 mmol). Isolated yield: 0.203 g (97%). <sup>1</sup>H NMR (CD<sub>3</sub>CN, 300 MHz, 25 °C): δ 8.22 (m, 3H; Pyr*H*<sub>m</sub> and Pyr*H*<sub>p</sub>), 6.92 (m, 4H; Ar*H*), 6.18 (m, 4H; Ar*H*), 2.58 ppm (s, 6H; N=CMe). <sup>13</sup>C{<sup>1</sup>H} NMR (CD<sub>3</sub>CN, 75 MHz, 25 °C): δ 180.5 (MeC=N), 162.1 (d, *J*<sub>CF</sub> = 246.7 Hz; C<sub>Ar</sub>), 160.0 (C<sub>Ar</sub>), 140.3 (d, *J*<sub>CF</sub> = 3.1 Hz; C<sub>Ar</sub>), 137.2 (C<sub>Ar</sub>), 128.6 (C<sub>Ar</sub>), 122.5 (d, *J*<sub>CF</sub> = 8.8 Hz; C<sub>Ar</sub>), 117.5 (d, *J*<sub>CF</sub> = 23.5 Hz; C<sub>Ar</sub>), 19.8 ppm (CH<sub>3</sub>). <sup>19</sup>F{<sup>1</sup>H} NMR (CD<sub>3</sub>CN, 282 MHz, 25 °C): δ -72.9 (d, *J*<sub>PF</sub> = 707.0 Hz; PF<sub>6</sub>), -114.5 (s; Ar-F). <sup>31</sup>P{<sup>1</sup>H} NMR (CD<sub>3</sub>CN, 121 MHz, 25 °C): δ -144.7 (q, *J*<sub>FP</sub> = 707.1 Hz; PF<sub>6</sub>). MS (ESI-TOF/MS, *m/z*) calcd for C<sub>42</sub>H<sub>34</sub>F<sub>4</sub>N<sub>6</sub>Fe [M + H]<sup>+</sup>, 753.2047; found 753.2069.

**Bis[2,6-bis(4-bromophenylimino)pyridine] iron(II) hexafluorophosphate (3c).** Procedure as for **3a** using: **2c** (0.188 g, 0.40 mmol) and FeCl<sub>2</sub> (0.25 g, 0.20 mmol). Isolated yield: 0.252 g (98%). <sup>1</sup>H NMR (CD<sub>3</sub>CN, 300 MHz, 25 °C): δ 8.24 (m, 3H; Pyr*H*<sub>m</sub> and Pyr*H*<sub>p</sub>), 7.33 (m, 4H; Ar*H*), 6.07 (m, 4H; Ar*H*), 2.59 ppm (s, 6H; N=CMe). <sup>13</sup>C{<sup>1</sup>H} NMR (CD<sub>3</sub>CN, 75 MHz, 25 °C): δ 180.9 (MeC=N), 160.2 (C<sub>Ar</sub>), 143.3 (C<sub>Ar</sub>), 137.3 (C<sub>Ar</sub>), 133.8 (C<sub>Ar</sub>), 129.0 (C<sub>Ar</sub>), 122.3 (C<sub>Ar</sub>), 122.0 (C<sub>Ar</sub>), 19.9 ppm (CH<sub>3</sub>). <sup>19</sup>F NMR (CD<sub>3</sub>CN, 282 MHz, 25 °C): δ -72.8 (d, *J*<sub>PF</sub> = 706.4 Hz; PF<sub>6</sub>). <sup>31</sup>P{<sup>1</sup>H} NMR (CD<sub>3</sub>CN, 121 MHz, 25 °C): δ -144.6 (q, *J*<sub>FP</sub> = 706.8 Hz; PF<sub>6</sub>). Anal. calcd for C<sub>42</sub>H<sub>34</sub>N<sub>6</sub>F<sub>12</sub>P<sub>2</sub>FeBr<sub>4</sub>: C, 39.16; H, 2.66. Found: C, 39.07; H, 2.79. MS (ESI-TOF/MS, *m/z*) calcd for C<sub>42</sub>H<sub>34</sub>Br<sub>4</sub>N<sub>6</sub>Fe [M + H]<sup>+</sup>, 992.8850; found 992.8894.

**Bis[2,6-bis(4-cyanophenylimino)pyridine] iron(II) hexafluorophosphate (3d).** Procedure as for **3a** using: **2d** (0.145 g, 0.40 mmol) and FeCl<sub>2</sub> (0.25 g, 0.20 mmol). Isolated yield: 0.208 g (97%). <sup>1</sup>H NMR (CD<sub>3</sub>CN, 300 MHz, 25 °C): δ 8.32 (m, 3H; Pyr*H*<sub>m</sub> and Pyr*H*<sub>p</sub>), 7.57 (d, 4H, *J*<sub>HH</sub> = 8.4 Hz; Ar*H*), 6.31 (m, 4H, *J*<sub>HH</sub> = 8.4 Hz; Ar*H*), 2.64 ppm (s, 6H; N=CMe). <sup>13</sup>C{<sup>1</sup>H} NMR (CD<sub>3</sub>CN, 75 MHz, 25 °C): δ 182.0 (MeC=N), 160.0 (C<sub>Ar</sub>), 147.2 (C<sub>Ar</sub>), 138.1 (C<sub>Ar</sub>), 135.2 (C<sub>Ar</sub>), 129.9 (C<sub>Ar</sub>), 121.6 (C<sub>Ar</sub>), 118.4 (C≡N), 112.5 (C<sub>Ar</sub>), 20.3 ppm (CH<sub>3</sub>). <sup>19</sup>F NMR (CD<sub>3</sub>CN, 282 MHz, 25 °C): δ -72.9 (d, *J*<sub>PF</sub> = 706.7 Hz; PF<sub>6</sub>). <sup>31</sup>P{<sup>1</sup>H} NMR (CD<sub>3</sub>CN, 121 MHz, 25 °C): δ -144.6 (q, *J*<sub>FP</sub> = 706.5 Hz; PF<sub>6</sub>). MS (ESI-TOF/MS, *m/z*) calcd for C<sub>46</sub>H<sub>34</sub>N<sub>10</sub>Fe [M + H]<sup>+</sup>, 783.2391; found 783.2053.

### Electrochemical methods

Cyclic voltammetry (CV) and differential pulse voltammetry (DPV) experiments were conducted using 0.6 mM of analyte dissolved in 15 mL dry CH<sub>3</sub>CN containing 0.1 M (*n*Bu<sub>4</sub>N)PF<sub>6</sub> and purged with Ar for 20 minutes prior to analysis. A CHI

760c bipotentiostat was employed, using a 3 mm diameter glassy carbon working electrode, a Ag/Ag<sup>+</sup> quasi-non-aqueous reference electrode separated by a Vycor tip, and a Pt wire counter electrode. CV experiments were conducted using scan rates of 50–800 mV s<sup>-1</sup>. DPV experiments were carried out using a 5 mV increment, 50 mV amplitude, 0.1 s pulse width, 0.0167 s sample width, and 0.5 s pulse period. Following analysis, ferrocene (FcH) was added to each solution as an internal standard, and potentials are reported *versus* the FcH<sup>0/+</sup> redox couple.<sup>41</sup>

Charging/discharging experiments were conducted *via* a chronopotentiometry protocol under an N<sub>2</sub> atmosphere using a reticulated vitreous carbon (RVC) working electrode (~700 cm<sup>2</sup>) in a glass cylindrical chamber (85 mL) containing an acetonitrile solution of both analyte and *n*Bu<sub>4</sub>PF<sub>6</sub> (0.3 M), and a Teflon-coated stirbar. A graphite rod counter electrode immersed in a 0.3 M *n*Bu<sub>4</sub>PF<sub>6</sub> solution was placed in a fritted tube (10 mL) separating the working and counter electrode chambers, and a fritted Ag/AgCl quasi-reference electrode placed into the working electrode chamber. Potential cut-offs were set to voltages at which the reversible couples for each analyte was observed to start and finish, according to CV experiments. Cycling experiments were executed at various anodic and cathodic currents, with a (dis)charge time of 3600 s, which corresponds to a 1C (dis)charging rate assuming a 2e<sup>-</sup> reduction process.

### X-Ray crystallography

Crystal structure data was using collected from a multi-faceted crystal of suitable size and quality selected from a representative sample of crystals of the same habit using an optical microscope. Each crystal was mounted on a MiTiGen loop and data collection carried out in a cold stream of nitrogen (150 K; Bruker D8 QUEST ECO; Mo K<sub>α</sub> radiation). All diffractometer manipulations were carried out using Bruker APEX3 software.<sup>42</sup> Structure solution and refinement was carried out in the OLEX2<sup>43</sup> program using XS, XT and XL software, as well as the Bruker SHELXTL suite.<sup>42</sup> For each structure, the absence of additional symmetry was confirmed using ADDSYM incorporated in the PLATON program.<sup>44</sup>

Crystal structure data for **1b** (CCDC 1983239<sup>†</sup>): X-ray quality single crystals were grown by cooling a concentrated CH<sub>3</sub>CN solution to -20 °C overnight. Yellow plates, C<sub>23</sub>H<sub>20</sub>Cl<sub>2</sub>F<sub>2</sub>N<sub>4</sub>Zn, 526.70 g mol<sup>-1</sup>, triclinic, space group *P* $\bar{1}$ ; *a* = 8.8832(3) Å, *b* = 12.6990(5) Å, *c* = 21.7752(8) Å,  $\alpha$  = 105.6760(10)°,  $\beta$  = 95.8720(10)°,  $\gamma$  = 94.3010(10)°, *V* = 2339.09(15) Å<sup>3</sup>; *Z* = 4,  $\rho_{\text{calcd}}$  = 1.496 g cm<sup>-3</sup>; crystal dimensions 0.27 × 0.24 × 0.07 mm; diffractometer Bruker D8 QUEST ECO CMOS; Mo K<sub>α</sub> radiation, 150.0 K,  $2\theta_{\text{max}}$  = 55.132°; 56 870 reflections, 10 800 independent (*R*<sub>int</sub> = 0.0757), intrinsic phasing; absorption coeff ( $\mu$  = 1.312 mm<sup>-1</sup>), absorption correction semi-empirical from equivalents (SADABS); refinement (against *F*<sub>o</sub><sup>2</sup>) with SHELXTL V6.1, 583 parameters, 0 restraints, *R*<sub>1</sub> = 0.0618 (*I* > 2σ) and *wR*<sub>2</sub> = 0.1038 (all data), Goof = 1.111, residual electron density 0.63/−0.53 e Å<sup>-3</sup>. Two CH<sub>3</sub>CN solvent molecules were successfully modeled within the asymmetric unit.

Crystal structure parameters for **1c** (CCDC 1983241<sup>†</sup>): X-ray quality single crystals were grown by cooling a concentrated CH<sub>3</sub>CN/DMSO (10:1) solution to -20 °C overnight. Yellow rods, C<sub>23</sub>H<sub>18.5</sub>Br<sub>2</sub>Cl<sub>2</sub>N<sub>3.5</sub>Zn, 627.99 g mol<sup>-1</sup>, triclinic, space group *P* $\bar{1}$ ; *a* = 12.9613(7) Å, *b* = 14.5938(6) Å, *c* = 15.1144(7) Å,  $\alpha$  = 92.855(2)°,  $\beta$  = 110.335(2)°,  $\gamma$  = 102.818(2)°, *V* = 2588.7(2) Å<sup>3</sup>; *Z* = 4,  $\rho_{\text{calcd}}$  = 1.611 g cm<sup>-3</sup>; crystal dimensions 0.70 × 0.24 × 0.18 mm; diffractometer Bruker D8 QUEST ECO CMOS; Mo K<sub>α</sub> radiation, 150.0 K,  $2\theta_{\text{max}}$  = 61.442°; 34 726 reflections, 15 756 independent (*R*<sub>int</sub> = 0.0702), intrinsic phasing; absorption coeff ( $\mu$  = 4.257 mm<sup>-1</sup>), absorption correction semi-empirical from equivalents (SADABS); refinement (against *F*<sub>o</sub><sup>2</sup>) with SHELXTL V6.1, 555 parameters, 0 restraints, *R*<sub>1</sub> = 0.0708 (*I* > 2σ) and *wR*<sub>2</sub> = 0.1345 (all data), Goof = 1.037, residual electron density 1.61/−1.16 e Å<sup>-3</sup>. One CH<sub>3</sub>CN solvent molecule was modeled successfully, however due to difficulties modeling remaining solvents, the SQUEEZE protocol imbedded in PLATON<sup>44</sup> was used to remove a solvent void of 249 Å<sup>3</sup> containing 101 e<sup>-</sup>.

Crystal structure parameters for **1d** (CCDC 1983240<sup>†</sup>): X-ray quality single crystals were grown by layering a concentrated CH<sub>3</sub>CN solution with Et<sub>2</sub>O and cooling to -5 °C. Yellow blocks; C<sub>25</sub>H<sub>20</sub>Cl<sub>2</sub>N<sub>6</sub>Zn 540.74 g mol<sup>-1</sup>, monoclinic, space group *P*2<sub>1</sub>/*c*; *a* = 7.7284(7) Å, *b* = 14.8601(13) Å, *c* = 22.4323(19) Å,  $\alpha$  =  $\gamma$  = 90°,  $\beta$  = 97.628(4)°, *V* = 2553.4(4) Å<sup>3</sup>; *Z* = 4,  $\rho_{\text{calcd}}$  = 1.407 g cm<sup>-3</sup>; crystal dimensions 0.280 × 0.160 × 0.110 mm;  $2\theta_{\text{max}}$  = 56.11°; 66 904 reflections, 6121 independent (*R*<sub>int</sub> = 0.0966, intrinsic phasing; absorption coeff ( $\mu$  = 1.196 mm<sup>-1</sup>), absorption correction semi-empirical from equivalents (SADABS); refinement (against *F*<sub>o</sub><sup>2</sup>) with SHELXTL V6.1, 310 parameters, 0 restraints, *R*<sub>1</sub> = 0.0656 (*I* > 2σ) and *wR*<sub>2</sub> = 0.1495 (all data), Goof = 1.219, residual electron density 0.85/−1.04 Å<sup>-3</sup>.

Crystal structure parameters for **3c** (CCDC 1983242<sup>†</sup>): X-ray quality single crystals were grown by layering isopropyl ether over an acetonitrile solution and placing it in the freezer. Purple blocks, C<sub>44</sub>H<sub>37</sub>Br<sub>4</sub>F<sub>12</sub>FeN<sub>7</sub>P<sub>2</sub>, 1329.23 g mol<sup>-1</sup>, monoclinic, space group *Cc*; *a* = 17.9244(7) Å, *b* = 17.5570(7) Å, *c* = 15.9880(6) Å,  $\alpha$  =  $\gamma$  = 90°,  $\beta$  = 102.194(2)°, *V* = 4917.9(3) Å<sup>3</sup>; *Z* = 4,  $\rho_{\text{calcd}}$  = 1.795 g cm<sup>-3</sup>; crystal dimensions 0.370 × 0.270 × 0.210 mm; diffractometer Bruker D8 QUEST ECO CMOS; Mo K<sub>α</sub> radiation, 150.0 K,  $2\theta_{\text{max}}$  = 61.234°; 79 707 reflections, 14 968 independent (*R*<sub>int</sub> = 0.0501), intrinsic phasing; absorption coeff ( $\mu$  = 3.708 mm<sup>-1</sup>), absorption correction semi-empirical from equivalents (SADABS); refinement (against *F*<sub>o</sub><sup>2</sup>) with SHELXTL V6.1, 637 parameters, 2 restraints, *R*<sub>1</sub> = 0.0356 (*I* > 2σ) and *wR*<sub>2</sub> = 0.0590 (all data), Goof = 1.048, residual electron density 0.50/−0.51 e Å<sup>-3</sup>. A CH<sub>3</sub>CN solvent molecule was modeled successfully within the asymmetric unit.

Crystal structure parameters for **3d** (CCDC 1983243<sup>†</sup>): X-ray quality single crystals were grown by layering isopropyl ether over an acetonitrile solution and placing it in the freezer. Purple plates. C<sub>50</sub>H<sub>40</sub>N<sub>12</sub>F<sub>12</sub>P<sub>2</sub>Fe, 1154.73 g mol<sup>-1</sup>, monoclinic, space group *P*2<sub>1</sub>/*n*; *a* = 11.5217(6) Å, *b* = 32.6571(16) Å, *c* = 13.8662(7) Å,  $\alpha$  =  $\gamma$  = 90°,  $\beta$  = 98.732(2)°, *V* = 5156.9(5) Å<sup>3</sup>; *Z* = 4,  $\rho_{\text{calcd}}$  = 1.487 g cm<sup>-3</sup>; crystal dimensions 0.23 × 0.22 ×

0.07 mm; diffractometer Bruker D8 QUEST ECO CMOS; Mo K $\alpha$  radiation, 150.0 K,  $2\theta_{\max} = 49.700^\circ$ ; 121 300 reflections, 8890 independent ( $R_{\text{int}} = 0.1056$ ), intrinsic phasing; absorption coeff ( $\mu = 0.447 \text{ mm}^{-1}$ ), absorption correction semi-empirical from equivalents (SADABS); refinement (against  $F_o^2$ ) with SHELXTL V6.1, 700 parameters, 0 restraints,  $R_1 = 0.0717$  ( $I > 2\sigma$ ) and  $wR_2 = 0.1611$  (all data), Goof = 1.087, residual electron density 1.29/−0.97 e  $\text{\AA}^{-3}$ . Two CH<sub>3</sub>CN solvent molecules were modeled successfully within the asymmetric unit.

## Conflicts of interest

There are no conflicts to declare.

## Acknowledgements

We are grateful to the Natural Sciences Engineering Research Council of Canada for a Discovery Grant to DEH (RGPIN-2014-03733); the Canadian Foundation for Innovation and Research Manitoba for an award in support of an X-ray diffractometer (CFI #32146); and the University of Manitoba for GETS support (JDB, DBN) and a VP-RI USRA (BKS). C. Kuss and P. K. Giesbrecht are thanked for helpful discussions.

## References

- P. V. Kamat, K. S. Schanze and J. M. Buriak, *ACS Energy Lett.*, 2017, **2**, 1368–1369.
- W. Wang and V. Sprenkle, *Nat. Chem.*, 2016, **8**, 204–206.
- Y. Huang, S. Gu, Y. Yan and S. F. Y. Li, *Curr. Opin. Chem. Eng.*, 2015, **8**, 105–113.
- M. Arbabzadeh, J. X. Johnson, G. A. Keoleian, P. G. Rasmussen and L. T. Thompson, *Environ. Sci. Technol.*, 2016, **50**, 1046–1055.
- S. M. Laramie, J. D. Milshtein, T. M. Breault, F. R. Brushett and L. T. Thompson, *J. Power Sources*, 2016, **327**, 681–692.
- G. L. Soloveichik, *Chem. Rev.*, 2015, **115**, 11533–11558.
- R. W. Hogue and K. E. Toghil, *Curr. Opin. Electrochem.*, 2019, **18**, 37–45.
- J. A. Suttill, J. F. Kucharyson, I. L. Escalante-Garcia, P. J. Cabrera, B. R. James, R. F. Savinell, M. S. Sanford and L. T. Thompson, *J. Mater. Chem. A*, 2015, **3**, 7929–7938.
- J. I. van der Vlugt, *Chem. – Eur. J.*, 2019, **25**, 2651–2662.
- T. Storr and R. Mukherjee, *Inorg. Chem.*, 2018, **57**, 9577–9579.
- P. J. Cabrera, X. Yang, J. A. Suttill, K. L. Hawthorne, R. E. M. Brooner, M. S. Sanford and L. T. Thompson, *J. Phys. Chem. C*, 2015, **119**, 15882–15889.
- P. J. Cabrera, X. Yang, J. A. Suttill, R. E. M. Brooner, L. T. Thompson and M. S. Sanford, *Inorg. Chem.*, 2015, **54**, 10214–10223.
- C. S. Sevov, S. L. Fisher, L. T. Thompson and M. S. Sanford, *J. Am. Chem. Soc.*, 2016, **138**, 15378–15384.
- C. Ding, H. Zhang, X. Li, T. Liu and F. Xing, *J. Phys. Chem. Lett.*, 2013, **4**, 1281–1294.
- A. Crawford, V. Viswanathan, D. Stephenson, W. Wang, E. Thomsen, D. Reed, B. Li, P. Balducci, M. Kintner-Meyer and V. Sprenkle, *J. Power Sources*, 2015, **293**, 388–399.
- G. M. Duarte, J. D. Braun, P. K. Giesbrecht and D. E. Herbert, *Dalton Trans.*, 2017, **46**, 16439–16445.
- D. Enright, S. Gambarotta, G. P. A. Yap and P. H. M. Budzelaar, *Angew. Chem., Int. Ed.*, 2002, **41**, 3873–3876.
- J. J. Kiernicki, P. E. Fanwick and S. C. Bart, *Chem. Commun.*, 2014, **50**, 8189–8192.
- A. M. Tondreau, S. C. E. Stieber, C. Milsmann, E. Lobkovsky, T. Weyhermüller, S. P. Semproni and P. J. Chirik, *Inorg. Chem.*, 2013, **52**, 635–646.
- B. M. Wile, R. J. Trovitch, S. C. Bart, A. M. Tondreau, E. Lobkovsky, C. Milsmann, E. Bill, K. Wieghardt and P. J. Chirik, *Inorg. Chem.*, 2009, **48**, 4190–4200.
- A. A. Antonov, N. V. Semikolenova, V. A. Zakharov, W. Zhang, Y. Wang, W.-H. Sun, E. P. Talsi and K. P. Bryliakov, *Organometallics*, 2012, **31**, 1143–1149.
- A. S. Ionkin, W. J. Marshall, D. J. Adelman, A. L. Shoe, R. E. Spence and T. Xie, *J. Polym. Sci., Part A: Polym. Chem.*, 2006, **44**, 2615–2635.
- M. Gasperini, F. Ragaini and S. Cenini, *Organometallics*, 2002, **21**, 2950–2957.
- B. L. Small, *Acc. Chem. Res.*, 2015, **48**, 2599–2611.
- M. C. Thompson and D. H. Busch, *J. Am. Chem. Soc.*, 1962, **84**, 1762–1763.
- D. H. Busch and N. A. Stephenson, *Coord. Chem. Rev.*, 1990, **100**, 119–154.
- A. A. Mikhailine, E. Kim, C. Dingels, A. J. Lough and R. H. Morris, *Inorg. Chem.*, 2008, **47**, 6587–6589.
- T. Simler, A. A. Danopoulos and P. Braunstein, *Dalton Trans.*, 2017, **46**, 5955–5964.
- E. C. Alyea and P. H. Merrell, *Synth. React. Inorg. Met.-Org. Chem.*, 1974, **4**, 535–544.
- A. W. Addison, T. N. Rao, J. Reedijk, J. van Rijn and G. C. Verschoor, *J. Chem. Soc., Dalton Trans.*, 1984, 1349–1356.
- I. B. Lozada, T. Murray and D. E. Herbert, *Polyhedron*, 2019, **161**, 261–267.
- B. de Bruin, E. Bill, E. Bothe, T. Weyhermüller and K. Wieghardt, *Inorg. Chem.*, 2000, **39**, 2936–2947.
- L. P. Hammett, *J. Am. Chem. Soc.*, 1937, **59**, 96–103.
- A. J. Bard and L. R. Faulkner, *Electrochemical methods: fundamentals and applications*, Wiley, New York, 2nd edn, 2001.
- J. Noack, N. Roznyatovskaya, T. Herr and P. Fischer, *Angew. Chem., Int. Ed.*, 2015, **54**, 9776–9809.
- X. Wei, W. Pan, W. Duan, A. Hollas, Z. Yang, B. Li, Z. Nie, J. Liu, D. Reed, W. Wang and V. Sprenkle, *ACS Energy Lett.*, 2017, **2**, 2187–2204.
- Y. Zhao and H. R. Byon, *Adv. Energy Mater.*, 2013, **3**, 1630–1635.

- 38 C. Xie, H. Zhang, W. Xu, W. Wang and X. Li, *Angew. Chem., Int. Ed.*, 2018, **57**, 11171–11176.
- 39 H. Roth, N. Romero and D. Nicewicz, *Synlett*, 2015, **27**, 714–723.
- 40 Z. Flisak and W.-H. Sun, *ACS Catal.*, 2015, **5**, 4713–4724.
- 41 N. G. Connelly and W. E. Geiger, *Chem. Rev.*, 1996, **96**, 877–910.
- 42 G. M. Sheldrick, *Acta Crystallogr., Sect. A: Found. Crystallogr.*, 2008, **64**, 112–122.
- 43 O. V. Dolomanov, L. J. Bourhis, R. J. Gildea, J. A. K. Howard and H. Puschmann, *J. Appl. Crystallogr.*, 2009, **42**, 339–341.
- 44 A. L. Spek, *Acta Crystallogr., Sect. D: Biol. Crystallogr.*, 2009, **65**, 148–155.